

# Numerical approximation of a phase-field surfactant model with fluid flow

Guangpu Zhu<sup>a</sup>, Jisheng Kou<sup>b</sup>, Shuyu Sun<sup>c, \*</sup>, Jun Yao<sup>a</sup>, and Aifen Li<sup>a, \*</sup>

<sup>a</sup>Research Center of Multiphase Flow in Porous Media, School of Petroleum Engineering, China University of Petroleum (East China), Qingdao 266580, China

<sup>b</sup>School of Mathematics and Statistics, Hubei Engineering University, Xiaogan 432000, Hubei, China.

<sup>c</sup>Computational Transport Phenomena Laboratory, Division of Physical Science and Engineering, King Abdullah University of Science and Technology, Thuwal 23955-6900, Kingdom of Saudi Arabia

## Abstract

Modelling interfacial dynamics with soluble surfactants in a multiphase system is a challenging task. Here, we consider the numerical approximation of a phase-field surfactant model with fluid flow. The nonlinearly coupled model consists of two Cahn-Hilliard type equations and incompressible Navier-Stokes equations. Using the Invariant Energy Quadratization (IEQ) approach, the governing system is transformed into an equivalent form, which allows the nonlinear potentials to be treated efficiently and semi-explicitly. By some subtle explicit-implicit treatments to stress and convective terms, we construct a first and a second-order time marching schemes, which are extremely efficient and easy-to-implement, for the transformed governing system. At each time step, the schemes involve solving a sequence of linear elliptic equations, and computations of phase variables, velocity and pressure are totally decoupled. We further establish a rigorous proof of unconditional energy stability for the semi-implicit schemes. Numerical results in both two and three dimensions are obtained, which demonstrate that the proposed schemes are accurate, efficient and unconditionally energy stable. Using our schemes, we investigate the effect of surfactants on droplet deformation and collision under a shear flow. The increase of surfactant concentration can enhance droplet deformation and inhibit droplet coalescence.

**Keywords:** Phase-field model; Surfactant; Energy stability; Cahn-Hilliard; Navier-Stokes

## 1. Introduction

Surfactants are usually amphiphilic compounds that can absorb as a monomolecular layer to the interface between fluids and reduce the interfacial tension significantly [1-4]. There are two main types of surfactants, insoluble surfactants and soluble surfactants [1]. Insoluble surfactants only absorb at the interface, while soluble surfactants exist both in the bulk phases and on the interface. The ability of surfactants to control interfacial tension has made them been widely used in many industrial processes, including the manufacture of cosmetics, food processing and oil recovery [5, 6]. Surfactants also play an important role in microsystem with the presence of interface [7, 8], where the capillary effect dominates the inertia of fluids. The presence of surfactants at the interface will significantly alter the dynamical behavior in the microfluidic devices.

The phase-field model has been used extensively with great successes and has become one of the major tools to resolve the motion of free interfaces between multiple material components [9-12]. Unlike sharp interface models [1, 13-20], the phase-field method utilizes an appropriate free energy functional [21-34], which determines the thermodynamics of a system, to resolve the interfacial dynamics, thus it has a firm physical basis for multiphase flows. In the pioneering work of Laradji et al., the phase field model was first used to study the dynamics of phase separation of in a binary systems containing surfactants [35]. Since then, a variety of phase-field surfactant

models (free energy functional) have been proposed and well investigated. Komura et al. observed a series of drawbacks of Laradji et al. model and proposed a different two-order-parameter time dependent Ginzburg-Landau model [36]. Theissen and Gompper slightly modified the local coupling term of Laradji et al. model to deal with the same solubility of surfactants in the bulk phases [37]. Samn and Graaf introduced the logarithmic Floy-Huggins potential to restrict the range of local concentration of surfactants [38, 39]. In [40], the authors analyzed the well-posedness of the model proposed by Samn and Graaf, and provided strong evidence that it was mathematically ill-posed for a large set of physically relevant parameters. They made critical changes to the model and substantially increased the domain of validity. This modified model will be used in this study. In [6], the authors introduced a new model that can recover the Langmuir and Frumkin adsorption isotherms at the equilibrium.

The free energy functional only determines the thermodynamics of a system, and hydrodynamics should also be incorporated into a dynamic multiphase system [38, 41-43]. Numerically, it is extremely difficult to develop unconditionally energy stable schemes [2, 3, 39, 44] for phase-field surfactant models of two-phase incompressible flow. The main difficulties [3, 12] include: (1) the strong nonlinear couplings between multiple phase field variables; (2) the coupling between velocity and multiple phase-field variables through convection terms and nonlinear stresses; (3) the stiffness issue from the interfacial thickness; (4) the coupling of the velocity and pressure through incompressibility constraint. Several attempts have been made to solve the multiphase system with surfactants, including the work of Samn and Graaf [38], Engblom et al. [40], Yun et al. [45], Garcke et al. [41], Teigen et al. [43], Liu and Zhang [6]. Although they have obtained some interesting results using different numerical methods, none of them can provide the energy stability for numerical schemes in theory. It has been observed that numerical schemes with energy instability may introduce an excessive amount of numerical dissipation near singularities, which in turn lead to large numerical errors, particularly for long time integration [12]. Therefore, the main purpose of this study is construct an efficient scheme with unconditional energy stability for the coupled phase-field surfactant model and the Navier-Stokes equations. The scheme should be accurate, totally decoupled and easy-to-implement (only need to solve a sequence of linear, elliptic equations). To develop such a scheme, the invariant energy quadratization (IEQ) method is adopted in this study. The IEQ approach [3, 46, 47] introduces a set of new variables to transform the free energy density into an invariant quadratic functional. The new transformed system is exactly equivalent to the original system, and all nonlinear terms can be treated semi-explicitly, which in turn produces a linear system. To the best of the author's knowledge, the proposed schemes here are the first linear, decoupled and energy stable schemes for the hydrodynamics coupled phase-field surfactant model.

The rest of this paper is organized as follows. In section 2, we describe a nonlinearly coupled phase-field surfactant model with fluid flow. In section 3, the governing system are transformed into a new equivalent system by using the IEQ approach. Then we construct an efficient, decoupled and energy stable scheme for the transformed system and carry out the energy estimates for the proposed scheme. Several 2D and 3D numerical examples are investigated in Section 4 and the paper is finally concluded in Section 5.

## 2. The governing equation

For a multiphase system with surfactants, we consider a typical binary fluid-surfactant phase field model introduced in [40]. The non-dimensional free energy of system  $E_{ps}$  reads:

$$E_{ps}(\phi, \rho) = E_1(\phi) + E_2(\rho) + \int \left( \frac{\rho\phi^2}{4\text{Ex}} - \frac{\rho(\phi^2 - 1)^2}{4} \right) d\Omega. \quad (2.1)$$

where  $E_1(\phi)$  is the Ginzburg-Landau type of Helmholtz free energy functional. The phase-field variable  $\phi$  is used to label the local densities of two fluids ( $\phi_{\pm} = \pm 1$  in the two homogeneous equilibrium phases). Cn is the Cahn number relating to the interfacial thickness.

$$E_1(\phi) = \int_{\Omega} \left( \frac{(\phi^2 - 1)^2}{4} + \frac{\text{Cn}^2}{4} |\nabla\phi|^2 \right) d\Omega,$$

The first term in  $E_1(\phi)$ , the double well bulk energy, promotes the two-phase separation. The square-gradient term contributes to the mixing of two phases. The competition between the two types of interaction creates a thin smooth transition layer between the two homogeneous equilibrium phases [12].

To represent the surfactant concentration in a multiphase system, another phase-field variable  $\rho$  is introduced and the relative energy reads:

$$\begin{cases} E_2(\rho) = \int_{\Omega} \text{Pi}G(\rho)d\Omega, \\ G(\rho) = \rho \log(\rho) + (1-\rho) \log(1-\rho), \end{cases}$$

where Pi is the temperature-dependent constant taking the role of a diffusion coefficient for  $\rho$ .  $G(\rho)$  is the logarithmic Flory-Huggins type energy potential restricting the value of  $\rho$  to be inside the domain of (0, 1).

The local coupling term  $\rho\phi^2/(4\text{Ex})$  in (2.1) penalizes free surfactants in the bulk phases and stabilizes the phase-field model [40]. The positive parameter Ex controls the bulk solubility. The special molecular composition of surfactants enables them to selectively absorb on the interface, and form a buffer zone to reduce the system energy [6]. The surface energy  $\rho(\phi^2-1)^2/4$  accounts for the high concentration of surfactants near the interface [40].

Through the functional derivatives of free energy functional  $E_{ps}$  with respect to phase-field variables  $\phi$  and  $\rho$ , we obtain the chemical potentials  $w_{\phi}$  and  $w_{\rho}$  can be obtained,

$$w_{\rho} = \text{Pi} \log\left(\frac{\rho}{1-\rho}\right) + \frac{1}{4\text{Ex}} \phi^2 - \frac{(\phi^2 - 1)^2}{4}, \quad (2.2)$$

$$w_{\phi} = -\phi + \phi^3 - \frac{\text{Cn}^2}{2} \Delta\phi + \frac{1}{2\text{Ex}} \rho\phi - \rho\phi(\phi^2 - 1), \quad (2.3)$$

The evolution of phase-field variables  $\phi$  and  $\rho$  can be described by the Cahn-Hilliard-type equations

$$\rho_t + \nabla \cdot (\mathbf{u}\rho) = \frac{1}{\text{Pe}_{\rho}} \nabla \cdot M_{\rho} \nabla w_{\rho}, \quad (2.4)$$

$$\phi_t + \nabla \cdot (\mathbf{u}\phi) = \frac{1}{\text{Pe}_{\phi}} \Delta w_{\phi}, \quad (2.5)$$

where  $\mathbf{u}$  is the velocity,  $\text{Pe}_{\psi}$  and  $\text{Pe}_{\phi}$  are Péclet numbers. As in [40], a degenerate mobility  $M_{\rho} = \rho(1-\rho)$  is introduced to combine with the logarithmic chemical potential  $w_{\rho}$ . Equations (2.2) -(2.5) are coupled to the hydrodynamic equations in the form

$$\mathbf{u}_t + \mathbf{u} \cdot \nabla \mathbf{u} - \frac{1}{\text{Re}} \Delta \mathbf{u} + \nabla p + \frac{1}{\text{ReCaCn}} (\phi \nabla w_{\phi} + \rho \nabla w_{\rho}) = 0, \quad (2.6)$$

$$\nabla \cdot \mathbf{u} = 0, \quad (2.7)$$

where  $p$  is the pressure,  $\text{Re}$  is the Reynolds number, and  $\text{Ca}$  is the Capillary number. For the domain  $\Omega$ , periodic boundary conditions or the following boundary conditions can be used to close the system:

$$\partial_{\mathbf{n}} \phi|_{\Gamma} = \partial_{\mathbf{n}} \rho|_{\Gamma} = \nabla \cdot \mathbf{w}_{\phi} \cdot \mathbf{n}|_{\Gamma} = \nabla \cdot \mathbf{w}_{\rho} \cdot \mathbf{n}|_{\Gamma} = \mathbf{u}|_{\Gamma} = \partial_{\mathbf{n}} p|_{\Gamma} = 0. \quad (2.8)$$

Equations (2.2)-(2.8) form the complete hydrodynamics coupled phase-field surfactant model. The total energy  $E_{tot}$  of the hydrodynamics system is a sum of the kinetic energy  $E_k$  together with the free energy  $E_{ps}$ :

$$E_{tot} = E_k + E_{ps} = \int_{\Omega} \left( \frac{\text{We}}{2} |\mathbf{u}|^2 + \frac{(\phi^2 - 1)^2}{4} + \frac{\text{Cn}^2}{4} |\nabla \phi|^2 + \text{Pi}G(\rho) + \frac{\rho \phi^2}{4\text{Ex}} - \frac{\rho(\phi^2 - 1)^2}{4} \right) d\Omega, \quad (2.9)$$

where  $\text{We} = \text{ReCaCn}$ .

Now we analyze the planar equilibrium profiles for surfactant concentration  $\rho$ , which is important for subsequent numerical simulations [40]. Considering the fact that the steady-state chemical potential is constant, we have  $w_{\rho b} = w_{\rho(x)}$

$$w_{\rho_b} = \text{Pi} \log \left( \frac{\rho_b}{1 - \rho_b} \right) + \frac{1}{4\text{Ex}} \phi_b^2 - \frac{(\phi_b^2 - 1)^2}{4}, \quad (2.10)$$

$$w_{\rho(x)} = \text{Pi} \log \left( \frac{\rho(x)}{1 - \rho(x)} \right) + \frac{1}{4\text{Ex}} \phi^2 - \frac{(\phi^2 - 1)^2}{4}, \quad (2.11)$$

where  $\rho_b$  is the surfactant concentration in the bulk phases  $\rho(\infty)$ , and  $\phi_b$  is the bulk value  $\phi(\infty)$ . Subtracting (2.10) from (2.11), and introducing the intermediate variable  $\rho_L(x)$ , we get the relation

$$\text{Pi} \log \rho_L(x) = -\frac{1}{4\text{Ex}} (\phi_b^2 - \phi^2) - \frac{1}{4} [(\phi_b^2 - \phi^2)(2 - \phi_b^2 - \phi^2)], \quad (2.12)$$

then the steady-state profiles for  $\rho$  can be obtained

$$\rho(x) = \frac{\rho_b}{\rho_b + \rho_L(x) - \rho_L(x)\rho_b}. \quad (2.13)$$

Since the bulk concentration  $\rho_b$  is small,  $\phi_b = \pm 1$  and  $\phi = 0$  on the interface of fluids, equations (2.13) and (2.12) can be simplified to [40]

$$\rho_s = \frac{\rho_b}{\rho_b + \rho_L}, \quad (2.14)$$

$$\text{Pi} \log \rho_L = -\frac{1}{4} \left( 1 + \frac{1}{\text{Ex}} \right). \quad (2.15)$$

where  $\rho_s$  is the equilibrium concentration of surfactants on the phase interface. Equation (2.14) is the typical Langmuir isotherm and  $\rho_L$  is the Langmuir adsorption constant. Given specific  $\text{Pi}$  (temperature-dependent constant) and  $\text{Ex}$ ,  $\rho_L$  can be obtained.

### 3. Numerical schemes

#### 3.1 Transformed governing system and its energy law

We now develop some efficient time marching schemes to solve the nonlinearly coupled phase-field surfactant model with fluid flow. These schemes should be accurate, totally decoupled,

unconditionally energy stable and easy-to-implement. From the numerical point of view, it is quite a challenging topic to construct such schemes. The main difficulties include (1) The strong nonlinear couplings between phase-field variables; (2) The treatment of nonlinear potentials, such as the Ginzburg-Landau double well potential and Flory-Huggins potential; (3) the nonlinear coupling terms between phase-field variables and velocity through stress and convective terms; (4) the coupling of velocity and pressure through the incompressibility constraint.

For the first two difficulties (1) and (2), the commonly used techniques, such as convex splitting and stabilization approaches, may not be optimal choices due to some imperfections [3, 48]. The convex splitting approach usually produces nonlinear schemes, thus the implementations are often complicated and the computational costs are high [48]. The schemes constructed by the stabilization method are linear, energy stable and easy-to-implement. However, its stability requires that the classical PDE solution and the numerical solution hold the maximum principle, which is very hard to prove [48]. Therefore, a novel IEQ approach in this study is adopted to deal with nonlinear terms, and it has been successfully applied to solve a large class of gradient flows [2, 3, 46, 47]. Most recently, the authors have applied the IEQ approach to the case of multiple nonlinearly coupled variables in [2, 3]. For the difficulty (3), the computations of phase-field variables and velocity are decoupled through a subtle implicit-explicit treatment. For difficulty (4), we use a classical projection method to decouple the computation of velocity and pressure.

Before using the IEQ approach to transform the governing system, we first regularize the logarithmic potential  $G(\rho)$  from the domain  $(0, 1)$  to  $(-\infty, +\infty)$ . For any  $\xi > 0$ , the regularized logarithmic potential [3, 49] can be written as

$$\hat{G}(\rho) = \begin{cases} \rho \ln \rho + \frac{(1-\rho)^2}{2\xi} + (1-\rho) \ln \xi - \frac{\xi}{2}, & \text{if } \rho \geq 1-\xi, \\ \rho \ln \rho + (1-\rho) \ln(1-\rho), & \text{if } \xi \leq \rho \leq 1-\xi, \\ (1-\rho) \ln(1-\rho) + \frac{\rho^2}{2\xi} + \rho \ln \xi - \frac{\xi}{2}, & \text{if } \rho \leq \xi. \end{cases} \quad (3.1)$$

When  $\xi \rightarrow 0$ ,  $\hat{G}(\rho) \rightarrow G(\rho)$ , and we consider the numerical solution to the model formulated with the regularized function  $\hat{G}(\rho)$ . The  $\hat{\cdot}$  is omitted in the notation for convenience.

The IEQ approach introduces a set of new variables to transform the nonlinear potentials into invariant quadratic forms. The new transformed system is exactly equivalent to the original system, and all nonlinear terms can be treated semi-explicitly. More precisely, we define two auxiliary variables

$$U = \phi^2 - 1, \quad V = \sqrt{G(\rho) + B}, \quad (3.2)$$

where  $B$  is a positive constant to ensure  $G(\rho) + B > 0$ , and  $B = 1$  is adopted in this study [3]. Then the free energy functional  $E_{ps}$  can be rewritten as

$$E_{ps}(\phi, \rho, U, V) = \int \left( \frac{U^2}{4} + \frac{Cn^2}{4} |\nabla \phi|^2 + \text{Pi} V^2 + \frac{\rho \phi^2}{4E_x} - \frac{\rho U^2}{4} \right) d\Omega - \text{Pi} B |\Omega|, \quad (3.3)$$

Note that the free energy functional  $E_{ps}$  is not changed due to the introduction of the zero term  $\text{Pi} B - \text{Pi} B$ . Thus, a new and an equivalent governing system can be obtained by using the variational approach

$$\rho_t + \nabla \cdot (\mathbf{u}\rho) = \frac{1}{\text{Pe}_\rho} \nabla \cdot M_\rho \nabla w_\rho, \quad (3.4a)$$

$$w_\rho = \text{Pi}H(\rho)V + \frac{\phi^2}{4\text{Ex}} - \frac{U^2}{4}, \quad (3.4b)$$

$$V_t = \frac{H(\rho)}{2} \rho_t, \quad (3.4c)$$

$$\phi_t + \nabla \cdot (\mathbf{u}\phi) = \frac{1}{\text{Pe}_\phi} \Delta w_\phi, \quad (3.4d)$$

$$w_\phi = -\frac{\text{Cn}^2}{2} \Delta \phi + \phi U + \frac{\rho \phi}{2\text{Ex}} - \rho U \phi, \quad (3.4e)$$

$$U_t = 2\phi \phi_t, \quad (3.4f)$$

$$\mathbf{u}_t + \mathbf{u} \cdot \nabla \mathbf{u} + \nabla p - \frac{1}{\text{Re}} \Delta \mathbf{u} + \frac{1}{\text{We}} (\phi \nabla w_\phi + \rho \nabla w_\rho) = 0, \quad (3.4g)$$

$$\nabla \cdot \mathbf{u} = 0, \quad (3.4h)$$

with periodic boundary conditions or

$$\partial_{\mathbf{n}} \phi^{n+1} \Big|_{\Gamma} = \partial_{\mathbf{n}} \rho^{n+1} \Big|_{\Gamma} = \nabla \cdot w_\phi^{n+1} \cdot \mathbf{n} \Big|_{\Gamma} = \nabla \cdot w_\rho^{n+1} \cdot \mathbf{n} \Big|_{\Gamma} = \mathbf{u}^{n+1} \Big|_{\Gamma} = \partial_{\mathbf{n}} p^{n+1} \Big|_{\Gamma} = 0,$$

where  $H(\rho) = G'(\rho) / \sqrt{G(\rho) + B}$ .

Then we derive the PDE energy law for the transformed system (3.4).

**Theorem 3.1.** The transformed governing system (3.4) satisfies the following energy dissipation law:

$$\frac{d}{dt} E_{\text{tot}}(\phi, \rho, U, V) = -\frac{1}{\text{Pe}_\phi} \int |\nabla w_\phi|^2 d\Omega - \frac{1}{\text{Pe}_\rho} \int |\sqrt{M_\rho} \nabla w_\rho|^2 d\Omega - \text{CaCn} \int |\nabla \mathbf{u}|^2 d\Omega \leq 0. \quad (3.5)$$

where

$$E_{\text{tot}}(\phi, \rho, U, V) = \int \left( \frac{\text{We}}{2} |\mathbf{u}|^2 + \frac{\text{Cn}^2}{4} |\nabla \phi|^2 + \frac{U^2}{4} + \text{Pi}V^2 + \frac{\rho \phi^2}{4\text{Ex}} - \frac{\rho U^2}{4} \right) d\Omega - \text{Pi}B|\Omega|.$$

**Proof.** The detailed derivation can refer to the Appendix A.

With the introduction of two auxiliary variables  $U$  and  $V$ , the phase-field surfactant model is transformed into an equivalent form. It can be observed that the transformed phase-field surfactant model of two-phase incompressible flow satisfies the exactly same energy dissipation law with the original system for the time-continuous case. In the next section, we will focus on constructing time-marching schemes for the transformed governing system.

## 3.2 Linear, decoupled and energy stable schemes

### 3.2.1 First-order scheme

For phase-field models, constructing efficient and easy-to-implement numerical schemes with energy stability is the main challenge in the numerical approximation [12]. Numerical schemes that do not respect the energy dissipation laws may be “overloaded” with an excessive amount dissipation near singularities, which in turn lead to large numerical errors, particularly for long time integration [12, 50]. Hence, to accurately simulate the interfacial dynamics with surfactants, it is

especially desirable to design schemes that satisfy the discrete energy laws. In this section, we present a first-order scheme with unconditional energy stability to solve the governing system (3.4).

Given  $\rho^n, \phi^n, V^n, U^n, \mathbf{u}^n$  and  $p^n$ , the scheme (3.6) calculates  $\rho^{n+1}, \phi^{n+1}, V^{n+1}, U^{n+1}, \mathbf{u}^{n+1}$  and  $p^{n+1}$  for  $n \geq 0$  in four steps.

**Step 1**, we update  $\rho^{n+1}$  and  $V^{n+1}$  by solving

$$\frac{\rho^{n+1} - \rho^n}{\delta t} + \nabla \cdot (\mathbf{u}_*^n \rho^n) - \frac{1}{\text{Pe}_\rho} \nabla \cdot M_\rho^n \nabla w_\rho^{n+1} = 0, \quad (3.6a)$$

$$w_\rho^{n+1} = \text{Pi} H^n V^{n+1} + \frac{(\phi^n)^2}{4\text{Ex}} - \frac{(U^n)^2}{4}, \quad (3.6b)$$

$$V^{n+1} - V^n = \frac{1}{2} H^n (\rho^{n+1} - \rho^n), \quad (3.6c)$$

$$\mathbf{u}_*^n = \mathbf{u}^n - \frac{\delta t \rho^n}{\text{We}} \nabla w_\rho^{n+1}, \quad (3.6d)$$

$$\partial_{\mathbf{n}} \rho^{n+1} \Big|_{\Gamma} = 0, \quad \partial_{\mathbf{n}} w_\rho^{n+1} \Big|_{\Gamma} = 0,$$

**Step 2**, updating  $\phi^{n+1}$  and  $U^{n+1}$  using

$$\frac{\phi^{n+1} - \phi^n}{\delta t} + \nabla \cdot (\mathbf{u}_{**}^n \phi^n) - \frac{1}{\text{Pe}_\phi} \Delta w_\phi^{n+1} = 0, \quad (3.6e)$$

$$w_\phi^{n+1} = -\frac{\text{Cn}^2}{2} \Delta \phi^{n+1} + \phi^n U^{n+1} + \frac{\rho^{n+1} \phi^{n+1}}{2\text{Ex}} - \frac{1}{2} \rho^{n+1} U^n (\phi^{n+1} + \phi^n), \quad (3.6f)$$

$$U^{n+1} - U^n = 2\phi^n (\phi^{n+1} - \phi^n), \quad (3.6g)$$

$$\mathbf{u}_{**}^n = \mathbf{u}_*^n - \frac{\delta t \phi^n}{\text{We}} \nabla w_\phi^{n+1}, \quad (3.6h)$$

$$\partial_{\mathbf{n}} \phi^{n+1} \Big|_{\Gamma} = 0, \quad \partial_{\mathbf{n}} w_\phi^{n+1} \Big|_{\Gamma} = 0,$$

**Step 3**, we update  $\tilde{\mathbf{u}}^{n+1}$  by solving

$$\begin{cases} \frac{\tilde{\mathbf{u}}^{n+1} - \mathbf{u}^n}{\delta t} - \frac{1}{\text{Re}} \Delta \tilde{\mathbf{u}}^{n+1} + \nabla p^n + (\mathbf{u}^n \cdot \nabla) \tilde{\mathbf{u}}^{n+1} + \frac{1}{\text{We}} (\phi^n \nabla w_\phi^{n+1} + \rho^n \nabla w_\rho^{n+1}) = 0, \\ \tilde{\mathbf{u}}^{n+1} \Big|_{\Gamma} = 0, \end{cases} \quad (3.6i)$$

**Step 4**, updating  $p^{n+1}$  and  $\mathbf{u}^{n+1}$  using [12]

$$\begin{cases} \frac{\mathbf{u}^{n+1} - \tilde{\mathbf{u}}^{n+1}}{\delta t} + \nabla (p^{n+1} - p^n) = 0, \\ \nabla \cdot \mathbf{u}^{n+1} = 0, \quad \mathbf{u}^{n+1} \cdot \mathbf{n} \Big|_{\Gamma} = 0. \end{cases} \quad (3.6j)$$

**Remark 3.2.1.** (1) Computations of phase-field variables  $\phi^{n+1}$  and  $\rho^{n+1}$ , velocity  $\mathbf{u}^{n+1}$  and pressure  $p^{n+1}$  are totally decoupled. Moreover, the scheme (3.6) involves solving only a sequence of linear elliptic equations at each time step, which indicates that it is efficient and easy-to-implement;

(2) Once we obtained  $\rho^{n+1}$  and  $\phi^{n+1}$ ,  $V^{n+1}$  and  $U^{n+1}$  can be explicitly calculated from equations (3.6c) and (3.6g), respectively. Namely, the introduction of two auxiliary variables  $V$  and  $U$  do not involve extra computation costs.

(3) Following the idea in [12, 51], two first-order stabilization terms are introduced in explicit convective velocities  $\mathbf{u}_*^n$  and  $\mathbf{u}_{**}^n$ , respectively. The stabilization terms play a dominant role in constructing the unconditionally energy stable scheme, and this can be observed clearly in the proof of energy stability;

(4) The step 4 can also be rewritten as

$$\begin{cases} -\Delta(p^{n+1} - p^n) = -\frac{1}{\delta t} \nabla \cdot \tilde{\mathbf{u}}^{n+1}, & \partial_n(p^{n+1} - p^n)|_{\Gamma} = 0, \\ \mathbf{u}^{n+1} = \tilde{\mathbf{u}}^{n+1} - \delta t \nabla(p^{n+1} - p^n). \end{cases} \quad (3.7)$$

Now, we carry out the energy estimates for the above scheme.

**Theorem 3.2.** The linear, decoupled scheme (3.6) is unconditionally energy stable, and satisfies the following discrete energy law:

$$E^{n+1} - E^n \leq -\frac{1}{\text{Pe}_\rho} \left\| \sqrt{M_\rho^n} \nabla w_\rho^{n+1} \right\|^2 - \frac{1}{\text{Pe}_\phi} \left\| \nabla w_\phi^{n+1} \right\|^2 - \delta t \text{CaCn} \left\| \nabla \tilde{\mathbf{u}}^{n+1} \right\|^2 \leq 0, \quad (3.8)$$

where

$$\begin{aligned} E^n &= \frac{\text{We}}{2} \left\| \mathbf{u}^n \right\|^2 + \frac{\delta t^2 \text{We}}{2} \left\| \nabla p^n \right\|^2 + \frac{\text{Cn}^2}{4} \left\| \nabla \phi^n \right\|^2 + \frac{1}{4} \left\| U^n \right\|^2 + \text{Pi} \left\| V^n \right\|^2 \\ &\quad + \frac{1}{4\text{Ex}} \left( \rho^n, |\phi^n|^2 \right) - \frac{1}{4} \left( \rho^n, |U^n|^2 \right) - \text{Pi} B L_x L_y, \end{aligned}$$

here  $\|\cdot\|$  denotes the  $L^2$ -norm in  $\Omega$ .

**Proof.** By taking the inner product of (3.6a) with  $\delta t w_\rho^{n+1}$ , we can easily derive that

$$\left( \rho^{n+1} - \rho^n, w_\rho^{n+1} \right) - \delta t \left( \mathbf{u}_*^n \rho^n, \nabla w_\rho^{n+1} \right) = -\frac{\delta t}{\text{Pe}_\rho} \left\| \sqrt{M_\rho^n} \nabla w_\rho^{n+1} \right\|^2, \quad (3.9)$$

By taking the inner product of (3.6b) with  $-(\rho^{n+1} - \rho^n)$ , we can derive that

$$\begin{aligned} -\left( \rho^{n+1} - \rho^n, w_\rho^{n+1} \right) &= -\text{Pi} \left( H^n V^{n+1}, \rho^{n+1} - \rho^n \right) - \frac{1}{4\text{Ex}} \left( |\phi^n|^2, \rho^{n+1} - \rho^n \right) \\ &\quad + \frac{1}{4} \left( |U^n|^2, \rho^{n+1} - \rho^n \right), \end{aligned} \quad (3.10)$$

Taking the inner product of (3.6c) with  $2\text{Pi} V^{n+1}$  to obtain

$$\text{Pi} \left( \left\| V^{n+1} \right\|^2 - \left\| V^n \right\|^2 + \left\| V^{n+1} - V^n \right\|^2 \right) = \text{Pi} \left( H^n V^{n+1}, \rho^{n+1} - \rho^n \right), \quad (3.11)$$

Summing up equations (3.9) - (3.11), we get

$$\begin{aligned} \text{Pi} \left( \left\| V^{n+1} \right\|^2 - \left\| V^n \right\|^2 + \left\| V^{n+1} - V^n \right\|^2 \right) &= \delta t \left( \mathbf{u}_*^n \rho^n, \nabla w_\rho^{n+1} \right) - \frac{\delta t}{\text{Pe}_\rho} \left\| \sqrt{M_\rho^n} \nabla w_\rho^{n+1} \right\|^2 \\ &\quad - \frac{1}{4\text{Ex}} \left( |\phi^n|^2, \rho^{n+1} - \rho^n \right) + \frac{1}{4} \left( |U^n|^2, \rho^{n+1} - \rho^n \right), \end{aligned} \quad (3.12)$$

By taking the inner product of (3.6e) with  $\delta t w_\phi^{n+1}$ , we have

$$\left( \phi^{n+1} - \phi^n, w_\phi^{n+1} \right) - \delta t \left( \mathbf{u}_{**}^n \phi^n, \nabla w_\phi^{n+1} \right) = -\frac{\delta t}{\text{Pe}_\phi} \left\| \nabla w_\phi^{n+1} \right\|^2, \quad (3.13)$$

By taking the inner product of (3.6f) with  $-(\phi^{n+1} - \phi^n)$ , we can derive that

$$\begin{aligned}
& -(\phi^{n+1} - \phi^n, w_\phi^{n+1}) = -\frac{\text{Cn}^2}{2}(\nabla\phi^{n+1}, \nabla\phi^{n+1} - \nabla\phi^n) - (U^{n+1}\phi^n, \phi^{n+1} - \phi^n) \\
& \quad - \frac{1}{2\text{Ex}}(\rho^{n+1}\phi^{n+1}, \phi^{n+1} - \phi^n) + \frac{1}{2}(\rho^{n+1}U^n(\phi^{n+1} + \phi^n), \phi^{n+1} - \phi^n) \\
& = -\frac{\text{Cn}^2}{4}(\|\nabla\phi^{n+1}\|^2 - \|\nabla\phi^n\|^2 + \|\nabla\phi^{n+1} - \nabla\phi^n\|^2) - (U^{n+1}\phi^n, \phi^{n+1} - \phi^n) \\
& \quad - \frac{1}{4\text{Ex}}\left[(\rho^{n+1}, |\phi^{n+1}|^2) - (\rho^{n+1}, |\phi^n|^2) + (\rho^{n+1}, |\phi^{n+1} - \phi^n|^2)\right] \\
& \quad + \frac{1}{4}\left[(\rho^{n+1}, |U^{n+1}|^2) - (\rho^{n+1}, |U^n|^2) - (\rho^{n+1}, |U^{n+1} - U^n|^2)\right],
\end{aligned} \tag{3.14}$$

where  $\rho^n$  is the surfactant concentration at the  $n$  step, which is between 0 and 1.

Taking the inner product of (3.6g) with  $U^{n+1}/2$  to obtain

$$\frac{1}{4}(\|U^{n+1}\|^2 - \|U^n\|^2 + \|U^{n+1} - U^n\|^2) = (U^{n+1}\phi^n, \phi^{n+1} - \phi^n), \tag{3.15}$$

Summing up equations (3.12) - (3.15), and dropping off some positive terms, we have

$$\begin{aligned}
& \frac{\text{Cn}^2}{4}(\|\nabla\phi^{n+1}\|^2 - \|\nabla\phi^n\|^2) + \frac{1}{4}(\|U^{n+1}\|^2 - \|U^n\|^2) + \text{Pi}(\|V^{n+1}\|^2 - \|V^n\|^2) \\
& \quad + \frac{1}{4\text{Ex}}\left[(\rho^{n+1}, |\phi^{n+1}|^2) - (\rho^n, |\phi^n|^2)\right] - \frac{1}{4}\left[(\rho^{n+1}, |U^{n+1}|^2) - (\rho^n, |U^n|^2)\right] \\
& \leq -\frac{\delta t}{\text{Pe}_\rho}\left\|\sqrt{M_\rho^n}\nabla w_\rho^{n+1}\right\|^2 - \frac{\delta t}{\text{Pe}_\phi}\|\nabla w_\phi^{n+1}\|^2 + \delta t(\mathbf{u}_*^n \rho^n, \nabla w_\rho^{n+1}) + \delta t(\mathbf{u}_{**}^n \phi^n, \nabla w_\phi^{n+1}),
\end{aligned} \tag{3.16}$$

We can derive from equations (3.6d) and (3.6h) that

$$\text{We}(\tilde{\mathbf{u}}^{n+1} - \mathbf{u}^n) + \delta t(\rho^n \nabla w_\rho^{n+1} + \phi^n \nabla w_\phi^{n+1}) = \text{We}(\tilde{\mathbf{u}}^{n+1} - \mathbf{u}_{**}^n), \tag{3.17}$$

Now, by taking the inner product of (3.6i) with  $2\delta t \text{We} \tilde{\mathbf{u}}^{n+1}$ , and using (3.17), we can derive that

$$\text{We}\left(\|\tilde{\mathbf{u}}^{n+1}\|^2 - \|\mathbf{u}_{**}^n\|^2 + \|\tilde{\mathbf{u}}^{n+1} - \mathbf{u}_{**}^n\|^2\right) + 2\delta t \text{CaCn} \|\nabla \tilde{\mathbf{u}}^{n+1}\|^2 + 2\delta t \text{We}(\nabla p^n, \tilde{\mathbf{u}}^{n+1}) = 0, \tag{3.18}$$

By taking the inner product of (3.6j) with  $2\delta t^2 \text{We} \nabla p^n$  and  $\mathbf{u}^{n+1}$  separately, we obtain

$$\delta t^2 \text{We}\left(\|\nabla p^{n+1}\|^2 - \|\nabla p^n\|^2 - \|\nabla p^{n+1} - \nabla p^n\|^2\right) = 2\delta t \text{We}(\tilde{\mathbf{u}}^{n+1}, \nabla p^n), \tag{3.19}$$

and

$$\text{We}\left(\|\mathbf{u}^{n+1}\|^2 + \|\tilde{\mathbf{u}}^{n+1} - \mathbf{u}^n\|^2\right) = \text{We}\|\tilde{\mathbf{u}}^{n+1}\|^2, \tag{3.20}$$

We also derive from (3.6j) that

$$\delta t^2 \text{We}\|\nabla p^{n+1} - \nabla p^n\|^2 = \text{We}\|\tilde{\mathbf{u}}^{n+1} - \mathbf{u}^n\|^2, \tag{3.21}$$

Combining equations (3.18) - (3.21), we get

$$\text{We}\left(\|\mathbf{u}^{n+1}\|^2 - \|\mathbf{u}_{**}^n\|^2 + \|\tilde{\mathbf{u}}^{n+1} - \mathbf{u}_{**}^n\|^2\right) + 2\delta t \text{CaCn} \|\nabla \tilde{\mathbf{u}}^{n+1}\|^2 + \delta t^2 \text{We}\left(\|\nabla p^{n+1}\|^2 - \|\nabla p^n\|^2\right) = 0, \tag{3.22}$$

By taking the inner product of (3.6d) with  $\mathbf{u}_*^n$ , we can easily derive that

$$\text{We}\left(\|\mathbf{u}_*^n\|^2 - \|\mathbf{u}^n\|^2 + \|\mathbf{u}_*^n - \mathbf{u}^n\|^2\right) = -2\delta t \text{We}(\rho^n \nabla w_\rho^{n+1}, \mathbf{u}_*^n), \tag{3.23}$$

Similarly, taking the inner product of (3.6h) with  $\mathbf{u}_*^n$  to derive

$$\text{We} \left( \|\mathbf{u}_*^n\|^2 - \|\mathbf{u}_*^n\|^2 + \|\mathbf{u}_*^n - \mathbf{u}_*^n\|^2 \right) = -2\delta t \text{We} (\phi^n \nabla w_\phi^{n+1}, \mathbf{u}_*^n), \quad (3.24)$$

Adding equations (3.22) - (3.24) together, and dropping off some positive terms, we get

$$\begin{aligned} & \frac{\text{We}}{2} \left( \|\mathbf{u}^{n+1}\|^2 - \|\mathbf{u}^n\|^2 \right) + \delta t \text{CaCn} \|\nabla \tilde{\mathbf{u}}^{n+1}\|^2 + \frac{\delta t^2 \text{We}}{2} \left( \|\nabla p^{n+1}\|^2 - \|\nabla p^n\|^2 \right) \\ & \leq -\delta t (\rho^n \nabla w_\rho^{n+1}, \mathbf{u}_*^n) - \delta t (\phi^n \nabla w_\phi^{n+1}, \mathbf{u}_*^n), \end{aligned} \quad (3.25)$$

Finally, combining (3.16) and (3.25), we arrive at

$$\begin{aligned} & \frac{\text{We}}{2} \left( \|\mathbf{u}^{n+1}\|^2 - \|\mathbf{u}^n\|^2 \right) + \frac{\delta t^2 \text{We}}{2} \left( \|\nabla p^{n+1}\|^2 - \|\nabla p^n\|^2 \right) + \frac{\text{Cn}^2}{4} \left( \|\nabla \phi^{n+1}\|^2 - \|\nabla \phi^n\|^2 \right) \\ & + \frac{1}{4} \left( \|U^{n+1}\|^2 - \|U^n\|^2 \right) + \text{Pi} \left( \|V^{n+1}\|^2 - \|V^n\|^2 \right) \\ & + \frac{1}{4\text{Ex}} \left[ (\rho^{n+1}, |\phi^{n+1}|^2) - (\rho^n, |\phi^n|^2) \right] - \frac{1}{4} \left[ (\rho^{n+1}, |U^{n+1}|^2) - (\rho^n, |U^n|^2) \right] \\ & \leq -\frac{\delta t}{\text{Pe}_\rho} \left\| \sqrt{M_\rho^n} \nabla w_\rho^{n+1} \right\|^2 - \frac{\delta t}{\text{Pe}_\phi} \left\| \nabla w_\phi^{n+1} \right\|^2 - \delta t \text{CaCn} \|\nabla \tilde{\mathbf{u}}^{n+1}\|^2 \leq 0, \end{aligned} \quad (3.26)$$

which implies the desired results.  $\square$

**Remark 3.2.2.** By using the IEQ approach, we first proposed a linear, totally decoupled and unconditionally energy stable scheme for a hydrodynamics coupled phase-field surfactant model. Unlike the traditional time stepping schemes, such as convex splitting and stabilization approaches, the IEQ method only requires the nonlinear parts of free energy potential are bounded from below, and it is not restricted to the specific forms of nonlinear parts [3]. In this study, it works well for the fourth-order double well potential and logarithmic Flory-Huggins potential. With the introduction of two auxiliary variables  $U$  and  $V$ , nonlinear potentials are transformed into quadratic forms, which provides the fundamental support for the linearization method.

We can also construct a linear, semi-coupled and energy stable scheme. For the presentation of simplicity, we only list the coupling part, and other parts refer to the scheme (3.6).

$$\frac{\rho^{n+1} - \rho^n}{\delta t} + \nabla \cdot (\mathbf{u}_*^n \rho^n) - \frac{1}{\text{Pe}_\rho} \nabla \cdot M_\rho^n \nabla w_\rho^{n+1} = 0, \quad (3.27a)$$

$$\frac{\phi^{n+1} - \phi^n}{\delta t} + \nabla \cdot (\mathbf{u}_*^n \phi^n) - \frac{1}{\text{Pe}_\phi} \Delta w_\phi^{n+1} = 0, \quad (3.27b)$$

$$\mathbf{u}_*^n = \mathbf{u}^n - \frac{\delta t \rho^n}{\text{We}} \nabla w_\rho^{n+1} - \frac{\delta t \phi^n}{\text{We}} \nabla w_\phi^{n+1}. \quad (3.27c)$$

The proof of energy stability is similar to that for **theorem 3.2**, thus we omit the detail here.

### 3.2.2 Second-order scheme

Schemes with unconditional energy stability remove constraints on the time step size from the stability point of view. Nonetheless, we should notice that larger time step will definitely introduce larger numerical errors. To use a time step size as large as possible while maintaining the desirable accuracy, more accurate and energy stable schemes are needed, e.g., second-order schemes. In this section, we extend the above first-order schemes to a second-order version based on the backward

differentiation formula with the Adam-Bashforth explicit interpolation [48].

Given  $\rho^{n-1}$ ,  $\phi^{n-1}$ ,  $U^{n-1}$ ,  $V^{n-1}$ ,  $\rho^n$ ,  $\phi^n$ ,  $V^n$ , and  $U^n$ , the scheme calculates  $\rho^{n+1}$ ,  $\phi^{n+1}$ ,  $U^{n+1}$  and  $V^{n+1}$  in two steps.

**Step 1**, Updating  $\rho^{n+1}$  and  $V^{n+1}$  using,

$$\begin{cases} \frac{3\rho^{n+1} - 4\rho^n + \rho^{n-1}}{2\delta t} + \nabla \cdot (\mathbf{u}_*^n \rho^*) = \frac{1}{\text{Pe}_\rho} \nabla \cdot (M_\rho^* \nabla w_\rho^{n+1}), \\ w_\rho^{n+1} = \text{Pi}H(\rho^*)V^{n+1} + \frac{(\phi^*)^2}{4\text{Ex}} - \frac{(U^*)^2}{4}, \\ \frac{3V^{n+1} - 4V^n + V^{n-1}}{2\delta t} = \frac{1}{2}H(\rho^*)\left(\frac{3\rho^{n+1} - 4\rho^n + \rho^{n-1}}{2\delta t}\right), \\ \mathbf{u}_*^n = \mathbf{u}^* - \frac{\delta t \rho^*}{\text{We}} \nabla w_\rho^{n+1}, \\ \partial_{\mathbf{n}} \rho^{n+1}|_\Gamma = 0, \quad \partial_{\mathbf{n}} w_\rho^{n+1}|_\Gamma = 0, \end{cases} \quad (3.28a)$$

**Step 2**, we update  $\phi^{n+1}$  and  $U^{n+1}$  by solving

$$\begin{cases} \frac{3\phi^{n+1} - 4\phi^n + \phi^{n-1}}{2\delta t} + \nabla \cdot (\mathbf{u}_{**}^n \phi^*) = \frac{1}{\text{Pe}_\phi} \Delta w_\phi^{n+1}, \\ w_\phi^{n+1} = -\frac{\text{Cn}^2}{2} \Delta \phi^{n+1} + \phi^* U^{n+1} + \frac{\rho^{n+1} \phi^{n+1}}{2\text{Ex}} - \frac{\rho^{n+1} U^* \phi^{n+1}}{2} - \frac{\rho^{n+1} U^* \phi^*}{2}, \\ \frac{3U^{n+1} - 4U^n + U^{n-1}}{2\delta t} = 2\phi^* \left( \frac{3\phi^{n+1} - 4\phi^n + \phi^{n-1}}{2\delta t} \right), \\ \mathbf{u}_{**}^n = \mathbf{u}_*^n - \frac{\delta t \phi^*}{\text{We}} \nabla w_\phi^{n+1}, \\ \partial_{\mathbf{n}} \phi^{n+1}|_\Gamma = 0, \quad \partial_{\mathbf{n}} w_\phi^{n+1}|_\Gamma = 0, \end{cases} \quad (3.28b)$$

**Step 3**, we update  $\tilde{\mathbf{u}}^{n+1}$  by solving

$$\begin{cases} \frac{3\tilde{\mathbf{u}}^{n+1} - 4\mathbf{u}^n + \mathbf{u}^{n-1}}{2\delta t} - \frac{1}{\text{Re}} \Delta \tilde{\mathbf{u}}^{n+1} + \nabla p^n + \frac{1}{\text{We}} (\phi^* \nabla w_\phi^{n+1} + \rho^* \nabla w_\rho^{n+1}) = 0, \\ \tilde{\mathbf{u}}^{n+1}|_\Gamma = 0, \end{cases} \quad (3.28c)$$

**Step 4**, updating  $p^{n+1}$  and  $\mathbf{u}^{n+1}$  using

$$\begin{cases} \Delta(p^{n+1} - p^n) = \frac{3}{2\delta t} \nabla \cdot \tilde{\mathbf{u}}^{n+1}, \quad \partial_{\mathbf{n}}(p^{n+1} - p^n)|_\Gamma = 0, \\ \mathbf{u}^{n+1} = \tilde{\mathbf{u}}^{n+1} - \frac{2\delta t}{3} \nabla(p^{n+1} - p^n). \end{cases} \quad (3.28d)$$

where

$$\begin{cases} \phi^* = 2\phi^n - \phi^{n-1}, \quad \rho^* = 2\rho^n - \rho^{n-1}, \quad U^* = 2U^n - U^{n-1}, \\ V^* = 2V^n - V^{n-1}, \quad \mathbf{u}^* = 2\mathbf{u}^n - \mathbf{u}^{n-1}, \quad M_\rho^* = 2M_\rho^n - M_\rho^{n-1}. \end{cases}$$

Nonlinearly coupled terms between phase-field variables present a huge challenge to carry out the energy estimates. Although the unconditional stability of the second-order scheme still needs to be proved, a series of numerical tests performed in section 4.1 have shown that the proposed second-order scheme is energy stable.

## 4 Numerical results

An efficient finite difference/volume method on staggered grids is used for the spatial discretization. The advection terms in the Cahn-Hilliard-type equations and Navier-Stokes equations are discretized by a composite high resolution scheme. More precisely, the fluxes at cell faces are evaluated with a MINMOD scheme [52, 53]. The composite high resolution scheme not only achieves the second-order accuracy, but also preserves the physical properties of convection. Details on the MINMOD scheme can be found in [53]. In this section, we conduct a series of numerical results to demonstrate that the proposed scheme is accurate, efficient and unconditionally energy stable.

#### 4.1 Droplet deformation under shear

We first use the shear flow case to test the accuracy of the proposed schemes. All simulations are conducted in a rectangular domain  $[0, 6] \times [0, 4]$  with periodic boundary conditions on the left and right sides, as shown in Figure 1(a). Equal but opposite velocities are prescribed on the top and bottom walls, respectively. Initially, a circular bubble with the radius of  $R=1$  locates in the center of the domain. The surfactant bulk concentration  $\rho_b$  is  $1 \times 10^{-4}$ . The bubble radius  $R$  and top wall moving velocity are chosen as the characteristic length and velocity, respectively. Other simulation parameters are as follows:

$$\text{Pe}_\phi = 10, \quad \text{Pe}_\rho = 100, \quad \text{Re} = 0.5, \quad \text{Ca} = 0.5, \quad \text{Cn} = 0.025, \quad \text{Ex} = 1, \quad \text{Pi} = 0.1227.$$

LS1 and LS2 are used to represent the first-order scheme (3.6) and second-order scheme (3.28), respectively. We use LS2 with a small time step size  $\delta t = 6.25 \times 10^{-5}$  to calculate the reference solutions due to the lack of exact solutions. To reduce the error related to spatial discretization as much as possible, a spatial resolution  $n_x = 324, n_y = 216$  is used in simulations. A series of time step sizes  $\delta t = 2 \times 10^{-3}, 1 \times 10^{-3}, 5 \times 10^{-4}, 2.5 \times 10^{-4}$  and  $1.25 \times 10^{-4}$  are chosen to calculate the  $L^2$ -norm errors and convergence orders for phase-field variables  $\phi$  and  $\rho$  at  $t = 0.5$ . Table 1 demonstrates that the schemes LS1 and LS2 achieve the first-order and second-order accuracy in time, respectively. Moreover, the second-order scheme LS2 gives better accuracy than the first-order scheme at the same time step size.

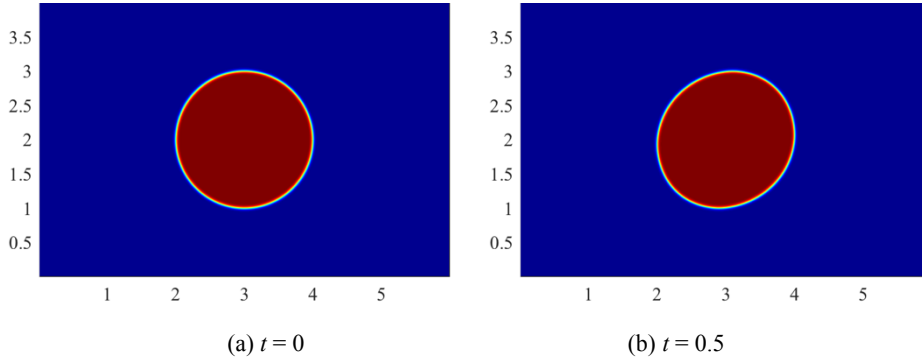


Figure 1 Time evolution of a droplet under a shear flow

**Table 1.** The  $L^2$  norm errors and convergence order for phase-field variables  $\phi$  and  $\rho$  at  $t = 0.5$  with different temporal resolutions.

$\Delta t$	LS1_ph	Order	LS1_tho	Order	LS2_ph	Order	LS2_tho	Order
2E-03	4.14E-02	—	1.73E-04	—	4.40E-03	—	6.53E-05	
1E-03	2.37E-02	0.81	1.05E-04	0.72	1.32E-03	1.74	1.88E-05	1.82
5E-04	1.21E-02	0.98	5.45E-05	0.95	3.52E-04	1.91	4.92E-06	1.91
2.5E-04	5.39E-03	1.16	2.45E-05	1.15	8.51E-05	2.05	1.22E-06	1.98
1.25E-4	1.83E-03	1.56	8.33E-06	1.56	2.12E-05	2.01	2.81E-07	2.07

Now we study the energy stability of the proposed schemes. To ensure no input energy from the outside, velocities of bottom and top walls  $\mathbf{u}_w$  are set to zero. Evolution of total free energy in Figure 2 confirms the energy stability of the proposed schemes. Considerable differences between different time step sizes can also be observed, indicating that the induced numerical errors with large time steps are higher.

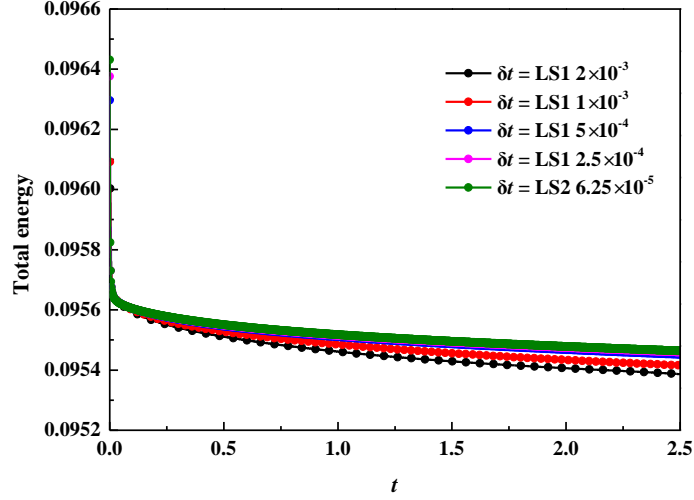


Figure 2 Energy curves at the different time step sizes. ( $\mathbf{u}_w = 0$ )

To examine the effect of surfactants, we consider three different surfactant bulk concentrations  $\rho_b = [1 \times 10^{-4}, 5 \times 10^{-3}, 1.5 \times 10^{-2}]$ . We use a grid size  $324 \times 216$  and time step size  $\delta t = 5 \times 10^{-4}$ . The aforementioned parameters will continue to be used in simulations. We run each simulation until  $t = 20$ . Figure 3 gives the evolution of a droplet under a shear flow with the presence of surfactants ( $\rho_b = 1.5 \times 10^{-2}$ ). It can be observed that surfactants gradually migrate towards to tip ends under the effect of shear flow. The movement of surfactants causes uneven distribution of interfacial tension, and the smallest interfacial tension occurs at the droplet tips. The non-uniform distribution of surfactants around the interface will lead to the increase of Marangoni force, which in turn prevents the migration of surfactants.

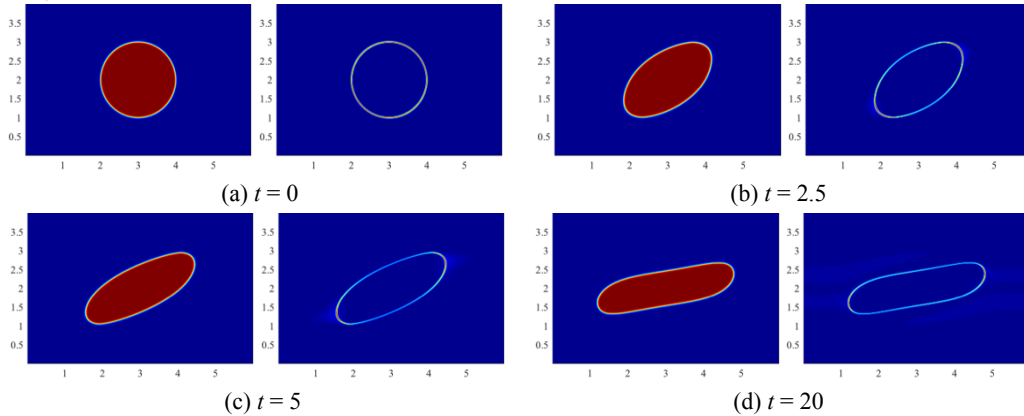


Figure 3 Time evolution of a droplet and surfactant concentration in a shear flow ( $\rho_b = 1.5 \times 10^{-2}$ ). For each subfigure, the left is the profile of  $\phi$ , and the right is the profile of  $\rho$ .

In Figure 4, we depict the droplet profiles at the different surfactant bulk concentrations  $\rho_b$ . As we expected, high surfactant bulk concentration results in a more prolate droplet, and differences

between droplet profiles increase with time. These results perfectly validate the effect of surfactants on reducing interfacial tension.

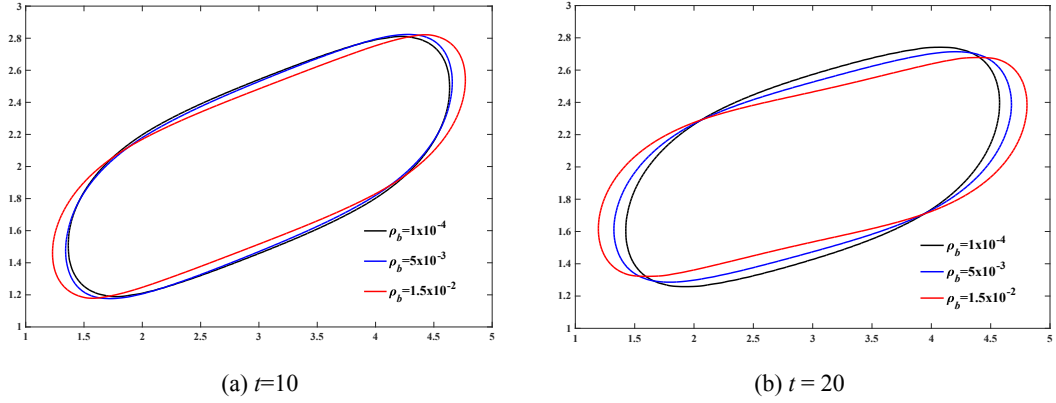


Figure 4 Time evolution of droplets under a shear flow with the presence of surfactants (black line:  $\rho_b=1\times 10^{-4}$ ; blue line:  $\rho_b=5\times 10^{-3}$ ; red line:  $\rho_b=1.5\times 10^{-2}$ ).

We continue to extend the study of droplet deformation to a three-dimensional domain  $\Omega = [0, 1] \times [0, 1] \times [0, 1]$ . We use a spatial resolution  $100\times 100\times 100$  and a time step-size  $\delta t = 5\times 10^{-4}$ .  $x$  and  $y$  directions are periodic boundaries. The side length of the domain and top wall moving velocity are chosen as the characteristic length and velocity, respectively. To facilitate the reader to reproduce the results, we list all paramters used in simulations:

$$Pe_\phi = 10, \quad Pe_\rho = 500, \quad Re = 10, \quad Ca = 0.2, \quad Cn = 0.015, \quad Ex = 1, \quad Pi = 0.1227.$$

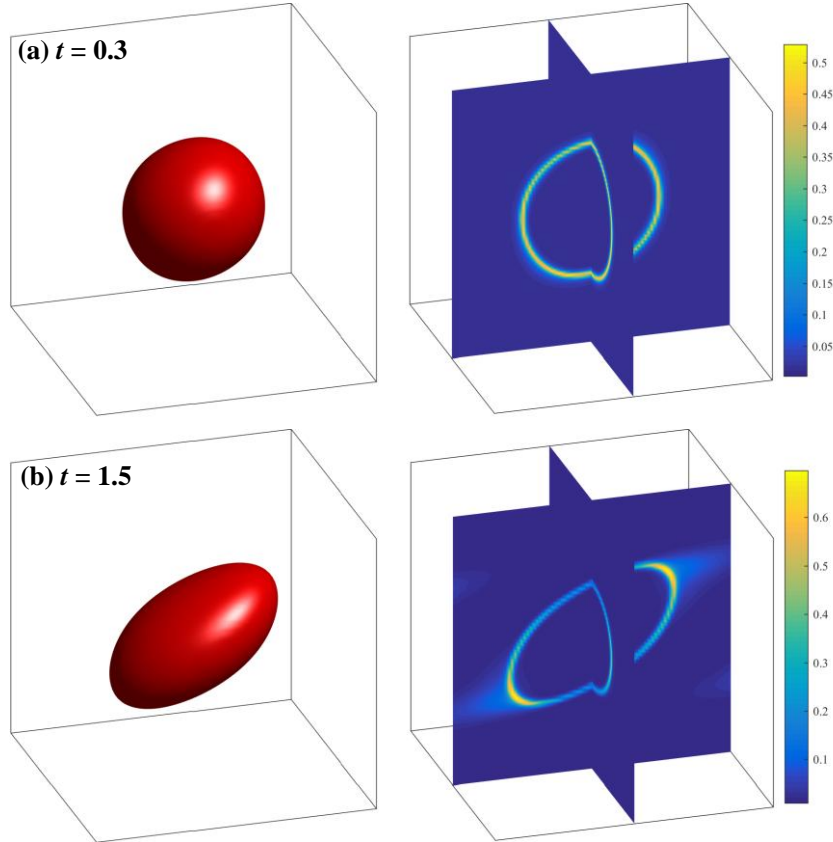


Figure 5 Time evolution of a droplet and surfactant concentration under the effect of shear flow ( $\rho_b=1.5\times 10^{-2}$ ). For each subfigure, the left is the profile of  $\phi$ , and the right is the profile of  $\rho$ .

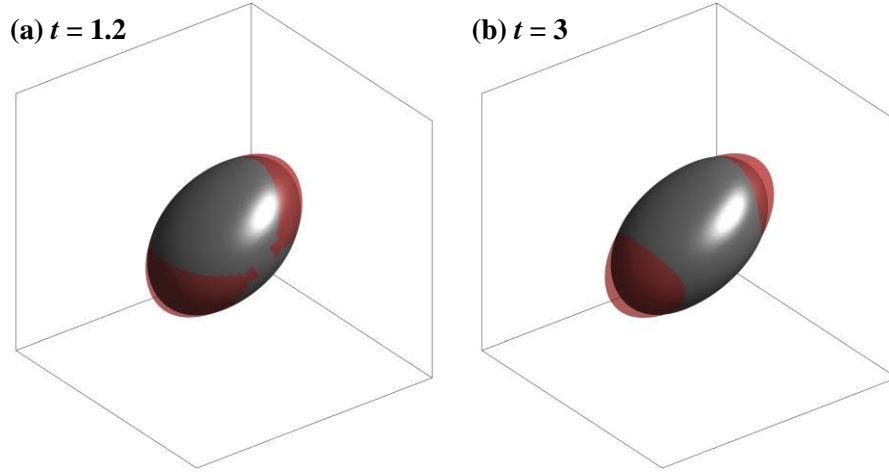


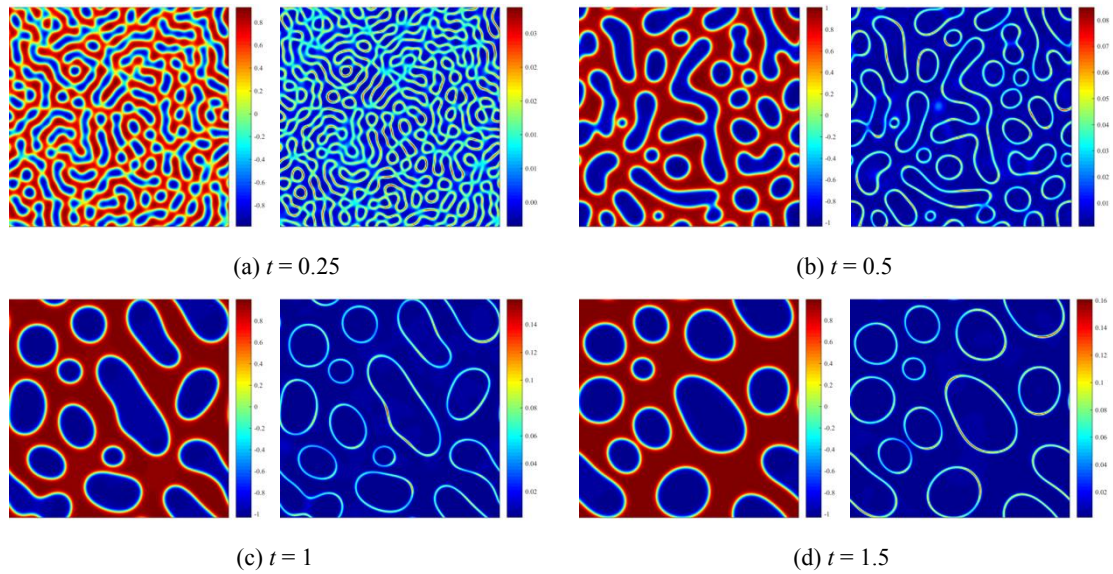
Figure 6 Evolutions of phase-field variable  $\phi$  in a shear flow at  $t = 1.2$  (left) and  $t = 3$  (right). (gray:  $\rho_b = 1 \times 10^{-4}$ ; red:  $\rho_b = 1.5 \times 10^{-2}$ )

Similar to the two-dimensional results, the droplet continuously deforms under the effect of shear flow and surfactants gradually swept towards to the tip ends of droplet (Figure 5a). Surfactants are convected into the bulk phases when the concentration of surfactants at the tip ends reach the maximum, as shown in Figure 5(b). Comparison of droplet profiles at the different surfactant bulk concentrations  $\rho_b$  is presented in Figure 6. Again, the results demonstrate the effect of surfactant in reducing surface tension.

#### 4.2. Coarsening Dynamics

To demonstrate the unconditional stability of the proposed numerical scheme, we use a 2D domain  $\Omega = [0, 1] \times [0, 1]$  to simulate the coarsening dynamics in the presence of flow. The initial conditions are taken as the randomly perturbed concentration fields:  $\phi = 0.1 + 0.001 \times \text{rand}(x, y)$ ,  $\rho = 0.01 + 0.001 \times \text{rand}(x, y)$ . The function  $\text{rand}(x, y)$  represents the random number in  $[0, 1]$ . All boundaries are periodic. We use a grid size of  $200^2$  and time step size of  $\delta t = 1 \times 10^{-4}$ . Other parameters used in simulations are listed as follows:

$$Pe_\phi = 100, \quad Pe_\rho = 100, \quad Re = 1, \quad Ca = 1, \quad Cn = 0.01, \quad Ex = 1, \quad Pi = 0.1227.$$



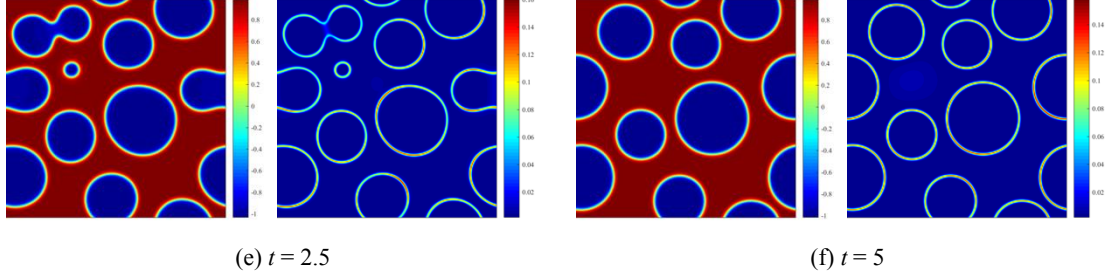


Figure 7 Evolution of the phase-field variables  $\phi$  and  $\rho$  at different times. For each subfigure, the left is the profile of  $\phi$ , and the right is the profile of  $\rho$ .

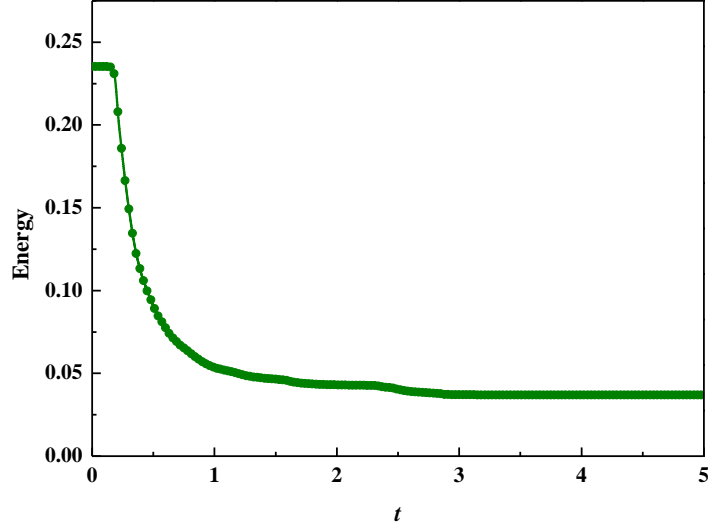


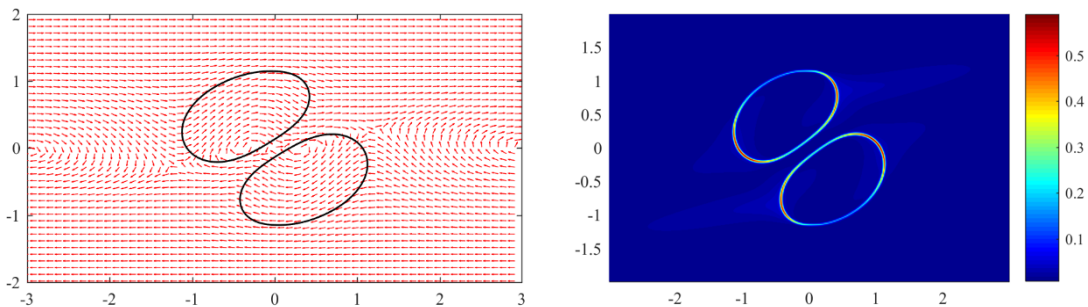
Figure 8 Time evolution of the total free energy  $E_{tot}$ .

Figure 7 gives the evolutions of phase-field variables  $\phi$  and  $\rho$  at different times. As we expected, surfactants are automatically absorbed to the interface of fluids. The energy curve in Figure 8 demonstrates that the proposed scheme is energy stable.

### 4.3 Colliding droplets

In this section, we perform the collision of two equal-sized droplets under a shear flow to investigate the effect of surfactants on droplet-droplet interactions. We conduct simulations on a  $6 \times 4$  flow domain with a spatial resolution  $360 \times 240$  and a time step-size  $\delta t = 5 \times 10^{-4}$ . Initially, two circular droplets with the radius of 0.7 locate at (1.5, 2.5) and (4.5, 1.5), respectively. The left and right sides of the domain are periodic boundary conditions. The detailed simulation parameters are as follows:

$$Pe_\phi = 10, \quad Pe_\rho = 100, \quad Re = 0.5, \quad Ca = 0.25, \quad Cn = 0.025, \quad Ex = 1, \quad Pi = 0.1227.$$



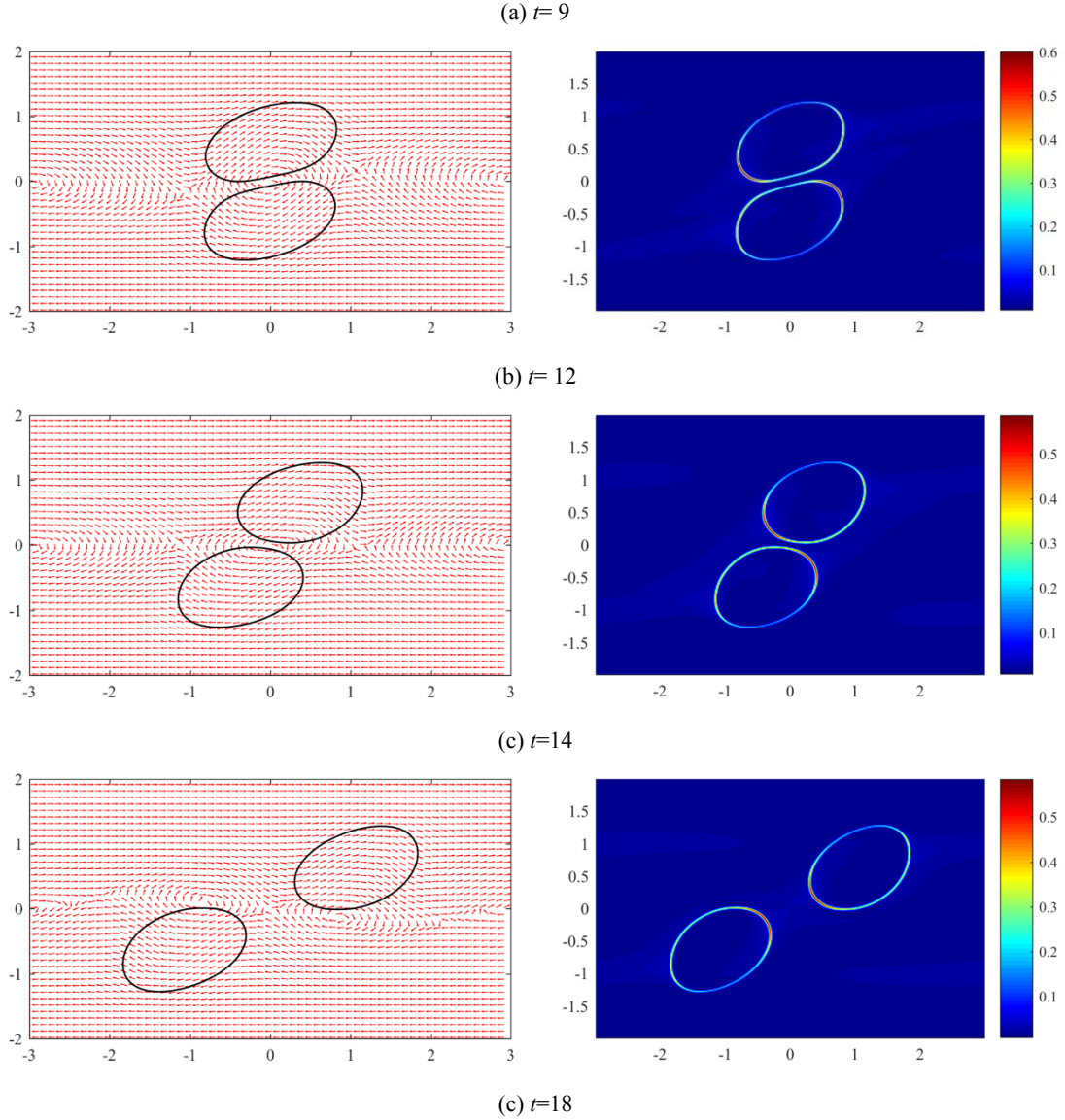


Figure 9 Evolution of two equal-sized droplets and surfactant concentration in a linear shear flow ( $\rho_b=1.5\times 10^{-2}$ ). For each subfigure, the left is the profile of  $\phi$ , and the right is the profile of  $\rho$ .

The left column of Figure 9 presents the evolution of two equal-sized droplets with high surfactant bulk concentration ( $\rho_b=1.5\times 10^{-2}$ ). The high surfactant bulk concentration prevents the droplet coalescence due to the collision, which is consistent with some experimental and numerical observations [8, 40]. The right column of figure 9 shows the concentration of surfactants. At the beginning, surfactants migrate towards the tips of each droplet. The pressure in the gap between two droplets sees a significant increase when the two droplets approach each other, which pushes surfactants away from the near-contact region, as shown in Figure 9(a) and Figure 9(b). Similarly, the uneven distribution of surfactants along the interface will arise the Marangoni force, which acts as an additional repulsive force to prevent droplet coalescence [6, 8]. Another non-negligible fact is that the presence of surfactants can enhance the deformation of droplet, and thus affect the collision process of droplets as well.

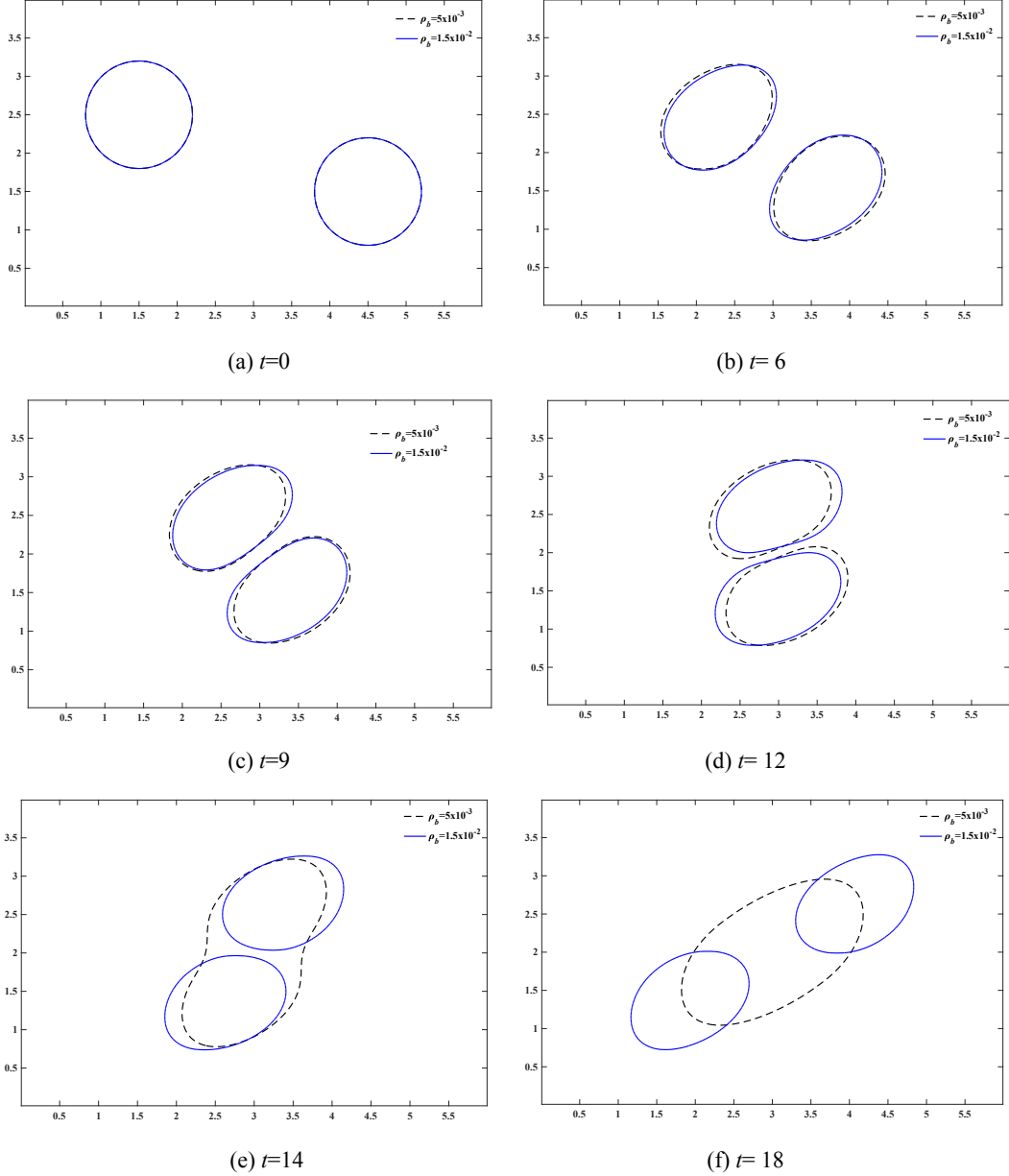


Figure 10 The collision of two droplets in a shear flow. (black dash line:  $\rho_b=5\times 10^{-3}$ ; blue solid line:  $\rho_b=1.5\times 10^{-2}$ )

Figure 10 compares the collision of two droplets at the different surfactant bulk concentrations under a shear flow. It can be observed that the two droplets collide and merge together at low surfactant concentration.

## 5 Conclusions

In this study, we simulate the interfacial dynamics with soluble surfactants in a multiphase system. Several linear, totally decoupled and energy stable schemes for a hydrodynamics coupled phase-field surfactant model are presented. Appropriate auxiliary variables are introduced to transform the governing system into an equivalent form, which allows the nonlinear potentials to be treated efficiently and semi-explicitly. At each time step, the schemes involve solving a sequence of linear elliptic equations, and computations of phase variables, velocity and pressure are totally decoupled. We also carry out the energy estimates for the semi-implicit schemes. Various two-dimensional and three-dimensional numerical experiments demonstrate that the surfactant concentration has significant impact on the droplet deformation and collision under a shear flow.

The increase in surfactant concentration can promote droplet deformation. The uneven distribution of surfactants along the interface will arise the Marangoni force, which acts as an additional repulsive force to prevent droplet coalescence.

### Acknowledgement

Jun Yao and Guangpu Zhu acknowledge that this work is supported by the National Science and Technology Major Project (2016ZX05011-001), the NSF of China (51490654, 51504276, and 51674280). The work of Shuyu Sun and Jisheng Kou is supported by the KAUST research fund awarded to the Computational Transport Phenomena Laboratory at KAUST through the Grant BAS/1/1351-01-01.

### Appendix A

In this section, we give the detailed derivation of the **Theorem 3.1**.

**Proof.** By taking the inner product of equation (3.4a) with  $w_\rho$ , we have,

$$(\rho_t, w_\rho) - (\rho \mathbf{u}, \nabla w_\rho) = -\frac{1}{\text{Pe}_\rho} \int |\sqrt{M_\rho} \nabla w_\rho|^2 d\Omega, \quad (\text{S.1})$$

where  $(\cdot, \cdot)$  is the inner product in  $L^2(\Omega)$ .

By taking the inner product of equation (3.4b) with  $-\rho_t$ , we can derive that

$$-(w_\rho, \rho_t) = -\text{Pi}(HV, \rho_t) - \frac{1}{4\text{Ex}}(\phi^2, \rho_t) + \frac{1}{4}(U^2, \rho_t), \quad (\text{S.2})$$

By taking the inner product of equation (3.4c) with  $2\text{Pi}V$ , we get

$$(V_t, 2\text{Pi}V) = \text{Pi} \frac{d}{dt} \int V^2 d\Omega = \text{Pi}(HV, \rho_t), \quad (\text{S.3})$$

Summing up equations (S.1) - (S.3), we obtain

$$\text{Pi} \frac{d}{dt} \int V^2 d\Omega - (\rho \mathbf{u}, \nabla w_\rho) = -\frac{1}{4\text{Ex}}(\phi^2, \rho_t) + \frac{1}{4}(U^2, \rho_t) - \frac{1}{\text{Pe}_\rho} \int |\sqrt{M_\rho} \nabla w_\rho|^2 d\Omega, \quad (\text{S.4})$$

By taking the inner product of equation (3.4d) with  $w_\phi$ , we get

$$(\phi_t, w_\phi) - (\mathbf{u}\phi, \nabla w_\phi) = -\frac{1}{\text{Pe}_\phi} \int |\nabla w_\phi|^2 d\Omega, \quad (\text{S.5})$$

By taking the inner product of equation (3.4e) with  $-\phi_t$ , we can derive that

$$\begin{aligned} -(w_\phi, \phi_t) &= \frac{\text{Cn}^2}{2}(\Delta\phi, \phi_t) - (\phi U, \phi_t) - \frac{1}{2\text{Ex}}(\rho\phi, \phi_t) + (\rho U\phi, \phi_t) \\ &= -\frac{\text{Cn}^2}{4} \frac{d}{dt} \int |\nabla\phi|^2 d\Omega - (\phi U, \phi_t) - \frac{1}{4\text{Ex}} \frac{d}{dt} \int \rho\phi^2 d\Omega + \frac{1}{4\text{Ex}}(\rho_t, \phi^2) \\ &\quad + \frac{1}{4} \frac{d}{dt} \int \rho U^2 d\Omega - \frac{1}{4}(\rho_t, U^2), \end{aligned} \quad (\text{S.6})$$

By taking the inner product of equation (3.4f) with  $U/2$ , we have

$$\frac{1}{2}(U_t, U) = \frac{1}{4} \frac{d}{dt} \int U^2 d\Omega = (\phi U, \phi_t), \quad (\text{S.7})$$

summing up equations (S.4) - (S.7), we obtain

$$\begin{aligned} &\frac{d}{dt} \int \frac{\text{Cn}^2}{4} |\nabla\phi|^2 + \frac{U^2}{4} + \text{Pi}V^2 + \frac{1}{4\text{Ex}} \rho\phi^2 - \frac{\rho U^2}{4} d\Omega \\ &= (\rho \mathbf{u}, \nabla w_\rho) + (\mathbf{u}\phi, \nabla w_\phi) - \frac{1}{\text{Pe}_\rho} \int |\sqrt{M_\rho} \nabla w_\rho|^2 d\Omega - \frac{1}{\text{Pe}_\phi} \int |\nabla w_\phi|^2 d\Omega, \end{aligned} \quad (\text{S.8})$$

By taking the inner product of equation (3.4g) with  $We\mathbf{u}$ , we have

$$\frac{We}{2} \frac{d}{dt} \int |\mathbf{u}|^2 d\Omega + CaCn \int |\nabla \mathbf{u}|^2 d\Omega - We(p, \nabla \cdot \mathbf{u}) + (\phi \mathbf{u}, \nabla w_\phi) + (\rho \mathbf{u}, \nabla w_\rho) = 0, \quad (S.9)$$

By taking the inner product of equation (3.4h) with  $We p$ , we can easily get

$$We(p, \nabla \cdot \mathbf{u}) = 0, \quad (S.10)$$

Summing up equations (S.8) - (S.10), we get the desired results (3.5)  $\square$

## References

- [1] S. Khatri, A.-K. Tornberg, An embedded boundary method for soluble surfactants with interface tracking for two-phase flows, *J. Comput. Phys.*, 256 (2014) 768-790.
- [2] X. Yang, Numerical Approximations for the Cahn–Hilliard Phase Field Model of the Binary Fluid-Surfactant System, *J. Sci. Comput.*, (2017) 1-21.
- [3] X. Yang, L. Ju, Linear and unconditionally energy stable schemes for the binary fluid–surfactant phase field model, *Computer Methods in Applied Mechanics and Engineering*, 318 (2017) 1005-1029.
- [4] I. Fonseca, M. Morini, V. Slastikov, Surfactants in foam stability: A phase-field model, *Arch. Ration. Mech. Anal.*, 183(3) (2007) 411-456.
- [5] S. Iglauer, Y. Wu, P. Shuler, Y. Tang, W.A. Goddard III, New surfactant classes for enhanced oil recovery and their tertiary oil recovery potential, *Journal of Petroleum Science and Engineering*, 71(1-2) (2010) 23-29.
- [6] H. Liu, Y. Zhang, Phase-field modeling droplet dynamics with soluble surfactants, *J. Comput. Phys.*, 229(24) (2010) 9166-9187.
- [7] M.-C. Lai, Y.-H. Tseng, H. Huang, Numerical simulation of moving contact lines with surfactant by immersed boundary method, *Communications in Computational Physics*, 8(4) (2010) 735.
- [8] H. Liu, Y. Ba, L. Wu, Z. Li, G. Xi, Y. Zhang, A hybrid lattice Boltzmann and finite difference method for droplet dynamics with insoluble surfactants, *J. Fluid Mech.*, 837 (2018) 381-412.
- [9] D. Jacqmin, Calculation of two-phase Navier–Stokes flows using phase-field modeling, *J. Comput. Phys.*, 155(1) (1999) 96-127.
- [10] J. Shen, X. Yang, A phase-field model and its numerical approximation for two-phase incompressible flows with different densities and viscosities, *SIAM. J. Sci. Compyt.*, 32(3) (2010) 1159-1179.
- [11] J. Shen, X. Yang, Numerical approximations of allen-cahn and cahn-hilliard equations, *Discrete Contin. Dyn. Syst*, 28(4) (2010) 1669-1691.
- [12] J. Shen, X. Yang, Decoupled, energy stable schemes for phase-field models of two-phase incompressible flows, *SIAM J. Numer. Anal.*, 53(1) (2015) 279-296.
- [13] A.J. James, J. Lowengrub, A surfactant-conserving volume-of-fluid method for interfacial flows with insoluble surfactant, *J. Comput. Phys.*, 201(2) (2004) 685-722.
- [14] M. Muradoglu, G. Tryggvason, A front-tracking method for computation of interfacial flows with soluble surfactants, *J. Comput. Phys.*, 227(4) (2008) 2238-2262.
- [15] L. Zhang, Q. Kang, J. Yao, Y. Gao, Z. Sun, H. Liu, A.J. Valocchi, Pore scale simulation of liquid and gas two-phase flow based on digital core technology, *Sci. China: Technol. Sci.*, 58(8) (2015) 1375-1384.
- [16] M. Booty, M. Siegel, A hybrid numerical method for interfacial fluid flow with soluble surfactant, *J. Comput. Phys.*, 229(10) (2010) 3864-3883.

- [17] J.-J. Xu, W. Ren, A level-set method for two-phase flows with moving contact line and insoluble surfactant, *J. Comput. Phys.* , 263 (2014) 71-90.
- [18] Z. Zhang, S. Xu, W. Ren, Derivation of a continuum model and the energy law for moving contact lines with insoluble surfactants, *Phys. Fluids*, 26(6) (2014) 062103.
- [19] J.-J. Xu, Z. Li, J. Lowengrub, H. Zhao, A level-set method for interfacial flows with surfactant, *J. Comput. Phys.* , 212(2) (2006) 590-616.
- [20] J.-J. Xu, Y. Yang, J. Lowengrub, A level-set continuum method for two-phase flows with insoluble surfactant, *J. Comput. Phys.* , 231(17) (2012) 5897-5909.
- [21] J. Kou, S. Sun, Multi-scale diffuse interface modeling of multi-component two-phase flow with partial miscibility, *J. Comput. Phys.* , 318 (2016) 349-372.
- [22] J. Kou, S. Sun, Unconditionally stable methods for simulating multi-component two-phase interface models with Peng–Robinson equation of state and various boundary conditions, *J. Comput. Appl. Math.* , 291 (2016) 158-182.
- [23] J. Kou, S. Sun, Thermodynamically consistent modeling and simulation of multi-component two-phase flow with partial miscibility, *Computer Methods in Applied Mechanics and Engineering*, 331 (2018) 623-649.
- [24] J. Kou, S. Sun, X. Wang, Linearly decoupled energy-stable numerical methods for multi-component two-phase compressible flow, arXiv preprint arXiv:1712.02222, (2017).
- [25] G. Zhu, H. Chen, S. Sun, J. Yao, A fully discrete energy stable scheme for a phase field moving contact line model with variable densities and viscosities, arXiv preprint arXiv:1801.08739, (2018).
- [26] G. Zhu, J. Yao, A. Li, H. Sun, L. Zhang, Pore-Scale Investigation of Carbon Dioxide-Enhanced Oil Recovery, *Energy Fuels*, 31(5) (2017) 5324-5332.
- [27] G. Zhu, J. Yao, L. Zhang, H. Sun, A. Li, B. Shams, Investigation of the Dynamic Contact Angle Using a Direct Numerical Simulation Method, *Langmuir*, 32(45) (2016) 11736-11744.
- [28] G.I. Tóth, B. Kvamme, Analysis of Ginzburg-Landau-type models of surfactant-assisted liquid phase separation, *Phys. Rev. E*, 91(3) (2015) 032404.
- [29] C.-H. Teng, I.-L. Chern, M.-C. Lai, Simulating binary fluid-surfactant dynamics by a phase field model, *Discrete and Continuous Dynamical Systems-Series B*, Special issue for FAN2010 in honor of J. Thomas Beale, in press, (2012).
- [30] H. Yu, X. Yang, Numerical approximations for a phase-field moving contact line model with variable densities and viscosities, *J. Comput. Phys.* , 334 (2017) 665-686.
- [31] P. Yue, J.J. Feng, C. Liu, J. Shen, A diffuse-interface method for simulating two-phase flows of complex fluids, *J. Fluid Mech.* , 515 (2004) 293-317.
- [32] X. Zheng, H. Babaei, S. Dong, C. Chrysosostomidis, G. Karniadakis, A phase-field method for 3D simulation of two-phase heat transfer, *Int. J. Heat Mass Transfer* 82 (2015) 282-298.
- [33] V. Voller, An enthalpy method for modeling dendritic growth in a binary alloy, *Int. J. Heat Mass Transfer* 51(3-4) (2008) 823-834.
- [34] R. Van Der Sman, Phase field simulations of ice crystal growth in sugar solutions, *Int. J. Heat Mass Transfer* 95 (2016) 153-161.
- [35] M. Laradji, H. Guo, M. Grant, M.J. Zuckermann, The effect of surfactants on the dynamics of phase separation, *J. Phys.: Condens. Matter* 4(32) (1992) 6715.
- [36] S. Komura, H. Kodama, Two-order-parameter model for an oil-water-surfactant system, *Phys. Rev. E*, 55(2) (1997) 1722.
- [37] O. Theissen, G. Gompper, Lattice-Boltzmann study of spontaneous emulsification, *The European*

- Physical Journal B-Condensed Matter and Complex Systems, 11(1) (1999) 91-100.
- [38] R. Van der Sman, S. Van der Graaf, Diffuse interface model of surfactant adsorption onto flat and droplet interfaces, *Rheol. Acta* 46(1) (2006) 3-11.
- [39] G. Zhu, J. Kou, S. Sun, J. Yao, A. Li, Decoupled, energy stable schemes for a phase-field surfactant model, *Comput. Phys. Commun.*, (2018).
- [40] S. Engblom, M. Do-Quang, G. Amberg, A.-K. Tornberg, On diffuse interface modeling and simulation of surfactants in two-phase fluid flow, *Communications in Computational Physics*, 14(4) (2013) 879-915.
- [41] H. Garcke, K.F. Lam, B. Stinner, Diffuse interface modelling of soluble surfactants in two-phase flow, *arXiv preprint arXiv:1303.2559*, (2013).
- [42] G. Pätzold, K. Dawson, Numerical simulation of phase separation in the presence of surfactants and hydrodynamics, *Phys. Rev. E*, 52(6) (1995) 6908.
- [43] K.E. Teigen, P. Song, J. Lowengrub, A. Voigt, A diffuse-interface method for two-phase flows with soluble surfactants, *J. Comput. Phys.*, 230(2) (2011) 375-393.
- [44] S. Gu, H. Zhang, Z. Zhang, An energy-stable finite-difference scheme for the binary fluid-surfactant system, *J. Comput. Phys.*, 270 (2014) 416-431.
- [45] A. Yun, Y. Li, J. Kim, A new phase-field model for a water-oil-surfactant system, *Applied Mathematics and Computation*, 229 (2014) 422-432.
- [46] X. Yang, L. Ju, Efficient linear schemes with unconditional energy stability for the phase field elastic bending energy model, *Computer Methods in Applied Mechanics and Engineering*, 315 (2017) 691-712.
- [47] X. Yang, J. Zhao, Q. Wang, J. Shen, Numerical approximations for a three-component Cahn-Hilliard phase-field model based on the invariant energy quadratization method, *Mathematical Models and Methods in Applied Sciences*, 27(11) (2017) 1993-2030.
- [48] X. Yang, H. Yu, Linear, second order and unconditionally energy stable schemes for a phase-field moving contact line model, *arXiv preprint arXiv:1703.01311*, (2017).
- [49] M. Copetti, C.M. Elliott, Numerical analysis of the Cahn-Hilliard equation with a logarithmic free energy, *Numerische Mathematik*, 63(1) (1992) 39-65.
- [50] U.S. Fjordholm, S. Mishra, E. Tadmor, Well-balanced and energy stable schemes for the shallow water equations with discontinuous topography, *J. Comput. Phys.*, 230(14) (2011) 5587-5609.
- [51] J. Shen, X. Yang, Decoupled energy stable schemes for phase-field models of two-phase complex fluids, *SIAM. J. Sci. Comput.*, 36(1) (2014) B122-B145.
- [52] J. Li, B. Yu, Y. Wang, Y. Tang, H. Wang, Study on computational efficiency of composite schemes for convection-diffusion equations using single-grid and multigrid methods, *J. Therm. Sci. Technol.*, 10(1) (2015) JTST0009-JTST0009.
- [53] F. Moukalled, L. Mangani, M. Darwish, The finite volume method in computational fluid dynamics, *An Advanced Introduction with OpenFOAM and Matlab*, (2016) 3-8.